Nonlinear multiscale modelling of quasi-solid state behaviour of PET/MWCNT nanocomposites: 3D RVE-based approach

Łukasz Figiel

International Institute for Nanocomposites Manufacturing (IINM), WMG, University of Warwick, Coventry, United Kingdom

Abstract

Nonlinear 3D RVE-based computational multiscale model for prediction of the quasi-solid state behaviour of PET/MWCNT nanocomposites is proposed in this work. The model links the time and length scale of representative morphology of the nanocomposite with the corresponding macroscopic scales via the numerical homogenisation. Finite Element simulations of the uniaxial extension of the nanocomposite near the glass transition show that the addition of MWCNTs leads to significant stiffening of PET. It is caused by an excellent reinforcing ability of the nanotubes, which on average are found to carry the load around two orders of magnitude larger than the matrix. A significant decrease of nanocomposite stresses with increasing processing temperature in its narrow range near the glass transition is also predicted by the model.

Keywords: Quasi-solid state processing, Multi-walled carbon nanotubes (MWCNTs), Nanocomposite, Multiscale modelling, Representative Volume Element (RVE)

1. Introduction

Subjecting entangled polymers to fast and large deformations near their glass transition is a common approach for manufacturing polymeric products. That approach can also be relatively easily adopted for polymers reinforced with nanoparticles [1-3]. During those processes polymers are in the semi-solid state and encounter complex nonlinear viscoelastic behaviour within, or near the temperature/time (rate) window between the glass transition and relaxation of entangled network (characterized by the time of tube disengagement by reptation). Thus, the polymer rheology is highly complex under these conditions, and for some entangled polymers it is further affected by structural instability under large deformations, which can cause stress-induced crystallization. Presence of nanoparticles in the polymer adds further complexity in

disturbing the rheological behaviour under processing conditions. Thus, advanced multiscale modelling of polymer nanocomposites can assist in providing more insight into the effects of nanoparticles on the polymer behaviour in the processing regime of interest. Then, it can also be used in simulations to find optimum material composition and optimum quasi-solid state processing conditions for polymer nanocomposites.

The rheological behaviour of entangled polymers and their nanocomposites under those conditions is challenging to capture with a mathematical model that can further be used in numerical simulations and optimization of the process. Several attempts have been made over the last two decades in developing models that capture the large deformation behaviour of unfilled entangled polymers under the conditions of interest [4-6]. However, there is only few attempts in describing the behaviour of nanofilled polymers in the same temperature and strain rate window. Particularly, the research has exclusively focussed on two-dimensional (2D) multiscale RVE-based modelling polymer nanocomposites with nanoplatelet-like reinforcement (i.e. nanoclay-filled polymers) [7-10]. However, the 2D RVE approach is unable to capture accurately the nanocomposite morphology and interactions between the nanotube-like nanoparticles and polymeric matrix, and thus it cannot describe correctly the stress transfer from the matrix to the nanotube across the interface.

Therefore, this work aims at developing a 3D multiscale nanocomposite model for predicting the effects of multi-walled carbon nanotubes (MWCNTs) on macroscopic behaviour of poly(ethylene terephthalate) (PET)/MWCNT nanocomposites just above the glass transition. It is achieved here by combining a 3D Representative Volume Element (RVE) concept with nonlinear homogenisation, and physically-based constitutive model for PET.

This communication starts with a short description of the multiscale model for the nanocomposite. It is then followed by the results and their discussion.

2. 3D RVE-based multiscale nanocomposite model

2.1. Multiscale modelling framework

An ultimate multiscale framework for a nanocomposite should link interactively length and time scales related to molecular interactions between the nanofiller and polymer matrix, nanofiller dispersion and distribution that define nanocomposite morphology, and macroscopic response, to provide accurate predictions of processing-structure-property

relationships for nanocomposites. However, the time scale of the current problem, which considers relaxation processes in the polymer matrix near the glass transition, extends well above nanoseconds. This is currently beyond capabilities of molecular dynamics (MD)-like simulations even when one considers a small nanoscale domain consisting of a single nanoparticle and a surrounding polymer. Thus, a two-scale approach of linking nanocomposite morphology and macro scales, enhanced with a physically-based model for the polymeric matrix to capture the aforementioned time-dependent processes, was pursued in this work. The approach used in this work is based on the Representative Volume Element (RVE) concept and the nonlinear homogenisation (coarse-graining) that generally enables the macro-to-RVE and RVE-to-macro transitions. For that it is assumed that the scale separation holds, and that the RVE is statistically representative of the entire nanocomposite morphology. Moreover, it is assumed that the macroscopic deformations are uniform, which justifies the use of the first-order homogenisation. Each material point at the macroscopic scale is assumed to be linked with an RVE, which represents explicitly the nanocomposite morphology i.e. distribution and dispersion of MWCNTs. Every material point is linked here to RVEs of the same morphology, which implies global periodicity.

The deformation at each macroscopic material point, which results from the macroscopic boundary conditions, is transferred onto a relevant RVE using the macroscopic deformation gradient $\boldsymbol{F}_{\mathrm{M}}$. Hence, current position of a point on the RVE boundary is represented by the position vector in the deformed configuration $\boldsymbol{x}_{\mathrm{RVE}}$, and it is driven by the macroscopic deformation gradient $\boldsymbol{F}_{\mathrm{M}}$ as follows:

$$\boldsymbol{x}_{\mathrm{RVE}} = \boldsymbol{F}_{\mathrm{M}} \boldsymbol{X}_{\mathrm{RVE}} + \boldsymbol{w}, \tag{1}$$

where $\boldsymbol{X}_{\mathrm{RVE}}$ is the position vector of the point in the undeformed configuration, while $\boldsymbol{w}$ is the fluctuation field arising from the nanocomposite morphology. Eq. (1) represents *macro-to-RVE* scale transition. Then, using $\boldsymbol{x}_{\mathrm{RVE}} = \boldsymbol{X}_{\mathrm{RVE}} + \boldsymbol{u}_{\mathrm{RVE}}$, Eq. (1) can be expressed in terms of displacements of the RVE faces

$$\boldsymbol{u}_{\mathrm{RVE}} = \left(\boldsymbol{F}_{\mathrm{M}} - \boldsymbol{1}\right) \boldsymbol{X}_{\mathrm{RVE}} + \boldsymbol{w}, \tag{2}$$

where $\boldsymbol{1}$ stands for the second-order identity matrix. The assumed periodicity of nanocomposite morphology leads to the following periodic boundary conditions

$$\boldsymbol{u}^{+}_{\mathrm{RVE}} - \boldsymbol{u}^{-}_{\mathrm{RVE}} = \left(\boldsymbol{F}_{\mathrm{M}} - \mathbf{1}\right)\left(\boldsymbol{X}^{+}_{\mathrm{RVE}} - \boldsymbol{X}^{-}_{\mathrm{RVE}}\right), \text{where } \boldsymbol{w}^{+} = \boldsymbol{w}^{-}, \tag{3}$$

where the subscripts '+' and '–' denote opposite faces of the RVE.

For the assumed kinematic scale transition and periodic boundary conditions, the deformation of an RVE leads to the stress response that is used to define the macroscopic Cauchy stress as

$$\boldsymbol{\sigma}_{\mathrm{M}} = \frac{1}{\mathrm{V}_{\mathrm{RVE}}} \int_{\mathrm{V}_{\mathrm{RVE}}} \boldsymbol{\sigma}_{\mathrm{RVE}}\left(\boldsymbol{x}_{\mathrm{RVE}}\right) \mathrm{dV}_{\mathrm{RVE}}, \tag{4}$$

where $\mathrm{V}_{\mathrm{RVE}}$ denotes the volume of the deformed RVE. Eq. (4) represents the *RVE-to-macro* scale transition. The multiscale approach for the PET/MWCNT nanocomposites is summarised in Fig. 1, and was integrated with the commercial FE software ABAQUS using its Python scripting and user-defined material (UMAT) subroutine.

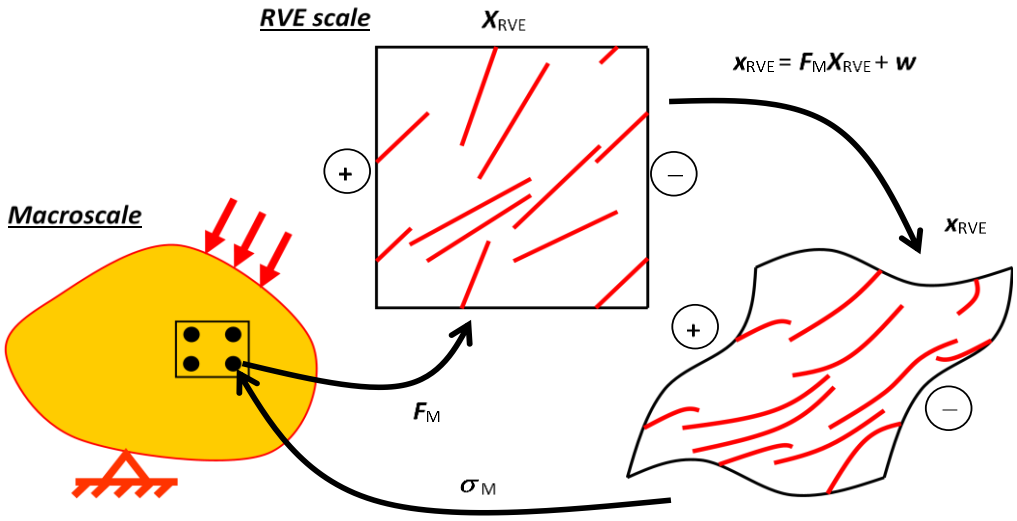

Fig. 1. *Nonlinear multiscale approach for PET-MWCNT nanocomposites based on the RVE concept and first-order nonlinear homogenisation*

2.2. Constitutive behaviour of nanocomposite constituents

The nonlinear multiscale approach is complemented by relevant constitutive laws for the PET and MWCNTs. A version of the glass-rubber model [4] modified with an empirical representation of tension-thinning of the PET flow, and described in detail elsewhere (see [8]), was used here to capture highly nonlinear, strain-, temperature- and time-dependent

behaviour of PET matrix in the nanocomposite. A unique feature of this model is its ability to capture the lock-up of viscous flow, which is manifested experimentally by the onset of strain hardening during stretching, and thus it is assumed here to be a precursor of the stress-induced crystallisation in PET. This 3D physically-based model combines stress contributions from intermolecular interactions (*bond-stretching* part, B) and conformational changes of an entangled polymeric network (*conformational part,* C) of PET. This results in the overall Cauchy stress tensor composed of deviatoric stress components B ($\hat{\boldsymbol{\sigma}}_B$) and C ($\hat{\boldsymbol{\sigma}}_C$), and the volumetric ($\sigma_m$) stress component, as follows:

$$\boldsymbol{\sigma} = \hat{\boldsymbol{\sigma}}_B + \hat{\boldsymbol{\sigma}}_C + \sigma_m \boldsymbol{1} \text{ , where } \sigma_m = K \ln J \tag{5}$$

where $\boldsymbol{1}$ is the second-order identity tensor, K is the bulk modulus, and J stands for the volume ratio. Full mathematical details of the modified glass-rubber model along with a full set of parameters are described in [8] (see Section 3 and Appendix A (the model), and Appendix C (the model parameters)). The model has been implemented as a UMAT subroutine in ABAQUS.

MWCNTs were approximated here as effective nanofibres because of computational efficiency of this description compared with the discrete representation of MWCNTs. Thus, the nanotubes were modelled using the effective linear elastic and transversely isotropic properties as in [10], using relevant closed-form formulas based on the molecular mechanics approach [11], and the replacement method proposed in [12]. For that purpose, perfectly straight MWCNTs were only considered in this work, where each wall of the MWCNT was assumed to exhibit an armchair structure. Additionally, external and internal diameters were taken as 15.5 and 4nm, respectively, which in combination with the interlayer distance of 0.34 nm, it provided a wall number of 18, which was used in the calculation of effective properties of the nanotubes. The full set of elastic constants used in the current work has been reported in Table 2 in reference [10] - see the column related to straight (effective) fibres under tension - it was assumed that the linear elastic response of a MWCNT in tension and compression is equal.

Perfect bonding at the interface between PET and MWCNTs was assumed in this communication for computational convenience. Clearly this is a significant simplification to the real situation where non-functionalised MWCNTs (as assumed here) may be weakly bonded with the surrounding polymeric matrix via van der Waals interactions. A more

realistic treatment of this problem would require development of an interfacial law and and/or a transition layer similarly to [10, 13] based on molecular mechanisms, to capture accurately polymer-nanotube interactions within the temperature range near the glass transition. Moreover, the behaviour of the polymer matrix near the nanotubes was assumed here to follow the same constitutive behaviour as the bulk polymer. Thus, the so called interphase polymer region around nanoparticles (see e.g. [14]) was not modelled in this work, due to the lack of experimental evidence.

2.3. Generation and FE meshing of RVEs

Acceptance rejection-algorithm was implemented in an in-house built Python-based script and used to populate 3D cubic RVEs with randomly distributed and randomly oriented effective nanofibres. In particular, RVEs were populated with ten (10) effective nanofibres at three volume fractions i.e. 0.1%, 0.3% and 0.5%. Those loadings correspond to typical values used in the experimental work [3]. It is noted that a small number (i.e. 10) of high-aspect ratio effective nanotubes was used in this communication purely due to computational efficiency. However, it must be noted that an insufficient number of inclusions such as nanotubes may lead to strong anisotropy, local or non-converged predictions of mechanical properties of heterogeneous systems, see e.g. [15]. For this, an extensive study of RVE size (deterministic size effects) and ensemble size (statistical size effects) should be carried out, see [16] – this was beyond the scope of this communication, and will be addressed in a more extensive contribution.

Free meshing algorithm built in the FE software ABAQUS was used in the discretisation of RVEs. Examples of RVEs meshed with FE software ABAQUS are shown in Fig. 2 - typical number of finite elements ranges from 120,000 to 200,000.

The domain of RVEs was divided into corners and faces to apply relevant boundary conditions (see Eqs. (2)-(3)). All translational degrees of freedom were constrained at one corner node of the RVE to prevent its rigid body motion. Displacements were applied to relevant corner nodes to simulate the macroscopic uniaxial extension of the nanocomposite. Those boundary conditions were complemented by the periodic boundary conditions, by tying relevant nodes on opposite faces of an RVE. A more detailed description of the boundary conditions can be found in [16], where uniaxial compression was considered.

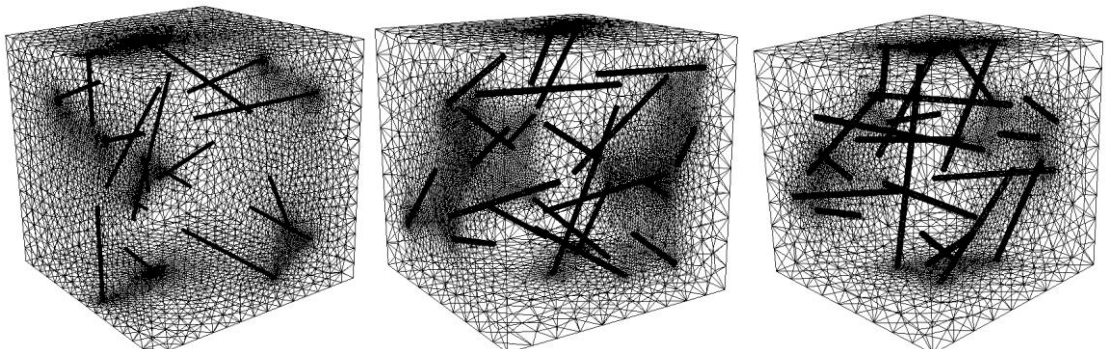

(a) 0.1% vol. (b) 0.3% vol. (c) 0.5% vol.

Fig. 2. *Examples of FE-meshed RVEs at different volume fractions of MWCNTs – each RVE contains 10 effective nanofibres of the aspect ratio 100, and of random orientation and random distribution*

3. Results and discussion

3D RVE-based FE simulations of uniaxial stretching of PET/MWCNTs were carried out at the applied strain rate 1 s^{-1} and temperatures within the quasi-solid state processing regime, i.e. 90 °C – 105 °C. Those conditions correspond to typical time-temperature window for the quasi-solid state processing of PET, and its nanocomposites. The uniaxial stretching regime up to the strain of around 0.5 corresponds to the experimental work of Mayoral et al. (2013). It must be mentioned though that in some cases the simulations were terminated earlier due to excessive local mesh distortions.

The macroscopic stress-strain behaviour of the nanocomposites was predicted as a function of the MWCNT content. Typical true stress-applied strain curves for the nanocomposite are shown in Fig. 3, where they are compared with the behaviour of the unfilled PET. Generally, the stress-strain curves for all the materials show qualitatively similar trends, where an initial nearly linear elastic response is followed by a gradual strain hardening behaviour. It must be noted that the simulations terminated due to excessive local finite element distortions within RVEs at different applied strains for different nanotube volume fractions. The 3D RVE-based simulations predicted strengthening of the polymer with the addition of the nanotubes, both at small and finite strains. The reinforcement effect is particularly pronounced at 0.5% nanotube loading, which significantly increases the nanocomposite stiffness. This is in qualitative agreement with the literature [3], where a significant reinforcement effect was found experimentally for PET reinforced with MWCNTs. Then, evaluation of the initial slope of the

predicted stress-strain curves yielded the following normalised values (i.e. slope of the stress-strain curve for the nanocomposite divided by the slope for the unfilled PET): ~1.09, ~1.11 and ~1.3 for the nanotube volume fractions 0.1%, 0.3% and 0.5%, respectively. It must be mentioned that these values are much smaller than those found experimentally for the PET/MWCNT nanocomposites [3]. This may suggest that the dispersion and distribution of nanotubes in PET nanocomposites in [3], differs from the one assumed in the current model - this requires further careful reconstruction of nanocomposite morphology, for example based on TEM images where actual aspect ratios and orientations can be determined. Another discrepancy between current simulations and experimental work in [3], may also result from the underestimation of mechanical properties of nanotubes and their aspect ratio. However, that was beyond this short communication, and will be accounted for in a more extended contribution. Moreover, the presence of nanotubes affects the stress relaxation of PET matrix in the nanocomposite – the value of stress at the transition point from the nearly linear elastic to viscoplastic regime increases with the nanotube content. The nanocomposite stiffening at finite strains is also connected with some reorientation of nanotubes as shown in Fig. 3 for a deformed RVE – in particular, some nanotubes tend to align with the applied load, and thus enhance the stress transfer from the matrix to the nano-reinforcement.

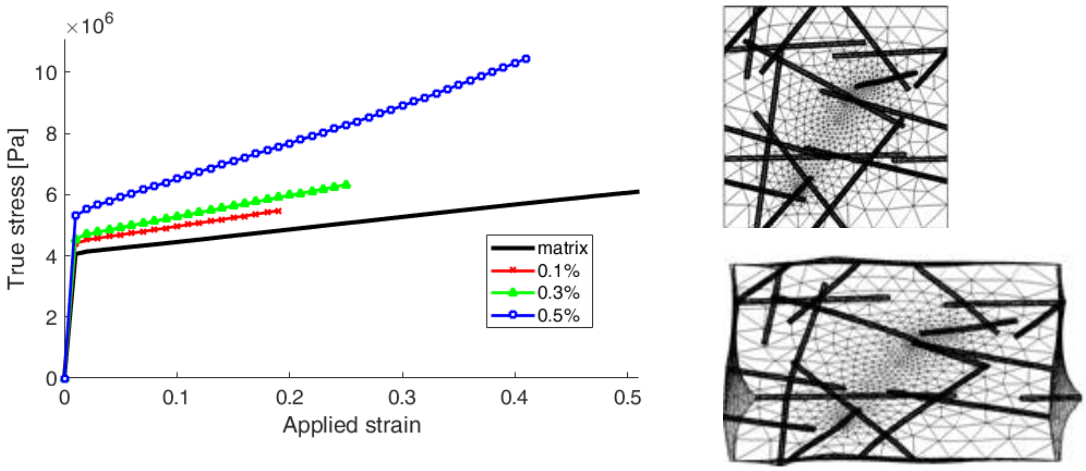

Fig. 3. *Representative macroscopic stress-strain curves for PET/MWCNT nanocomposites for different nanoparticle volume fractions – T=95 ℃, strain rate 1s^{-1} (left); 2D views of the undeformed and uniaxially deformed (at applied strain ε=0.41) RVEs for nanotube volume fraction 0.5% (right)*

The current multiscale approach also enables to apportion contributions from the matrix and nano-reinforcement. Thus, averaged stress-strain curves for those two nanocomposite phases were extracted from simulation results to obtain more insight into their contributions to the overall stress-strain response of the nanocomposite. A volume-averaging technique carried out separately for the matrix and nanotube phases led to the prediction of true stress components in the direction of the applied extension. The results are shown in Fig. 4.

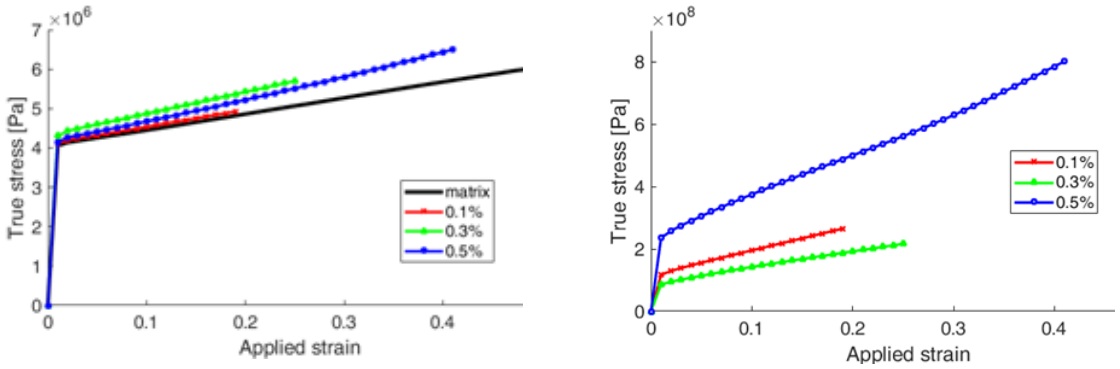

(a) (b)

Fig. 4. *Averaged stress-strain curves for nanocomposite phases for different nanotube volume fractions: (a) matrix phase; (b) nanotube phase – T=95 ℃, strain rate 1s^{-1}*

Strain amplification within the nano-filled PET matrix was predicted and assessed by the initial normalised slope, similarly as for the nanocomposite above – it resulted in ~1.07, ~1.52 and ~1.32 for 0.1%, 0.3% and 0.5% nanotube contents, respectively. It is believed that the strain amplification for 0.3% is slightly higher than for 0.5%, because of a specific arrangement of nanotubes, which enhance local strain in the nanocomposite matrix more efficiently for 0.3%. This is confirmed by the stress-strain curves obtained for the entire nanotube phase in the direction of extension. Here, one can see that the stress transfer from the matrix to the nanotube phase for 0.3% of nanotube loading is not as efficient as for volume fractions 0.1% and 0.5%. In addition, it must be noted that the MWCNT phase was predicted to carry the stress, which is around two orders of magnitude larger than the one carried by the matrix, and the nanocomposite.

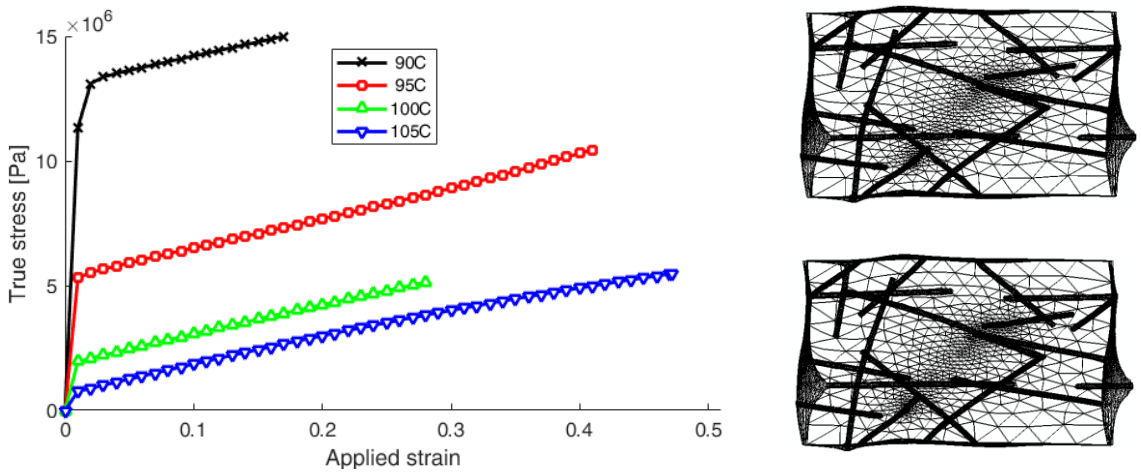

Fig. 5. *Representative stress-strain curves for the nanocomposites at different processing temperatures – nanotube content 0.5 % vol., strain rate 1s^{-1} (left); 2D views of uniaxially deformed RVEs (applied strain ε=0.41) at T=95 ℃ (top right) and 105 ℃ (bottom right)*

The magnitude of stresses experienced during quasi-solid state processing can affect the product shape (stability of the form during processing) and the energy input into the process. However, the stress level can be controlled via processing conditions such as temperature or strain rate. Therefore, the stress-strain curves were predicted as a function of temperature within the quasi-solid state processing regime i.e. just above the glass transition, for the MWCNT volume fraction of 0.5%. The sensitivity of the nanocomposite response to temperature is significant - the stresses are strongly affected by the processing temperature within its narrow range as shown in Fig. 5 - the magnitude of stresses in the nanocomposite decreases more than twice with the temperature increment of 5°C. However, those macroscopic results were not reflected in major differences in morphology evolution of nanocomposites as shown for two RVEs at 95°C and 105°C in Fig. 5 (right). Similarly to the stress-strain curves for different nanotube volume fractions, the excessive finite element distortions resulted in simulations terminating at different strains for different processing temperatures.

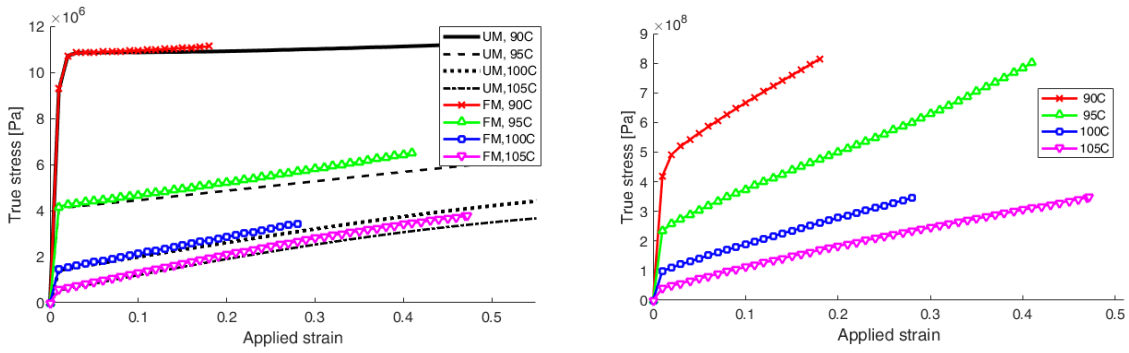

(a) (b)

Fig. 6. *Averaged stress-strain curves for nanocomposite phases at different processing temperatures: (a) matrix phase* (UM – unfilled matrix; FM – filled matrix)*; (b) nanotube phase – T=95℃, strain rate* $1s^{-1}$

The effect of processing temperature on averaged stresses resulting from separate contributions from the matrix (in the nanocomposite) and nanotube phases was also investigated. The stresses in the nanocomposite matrix were significantly affected by the processing temperature as shown in Fig. 6a – they increased with decreasing temperature in a similar manner as for the entire nanocomposite. However, the stress amplification in the nanocomposite matrix brought by the presence of nanotubes was less significant for different temperatures, as compared with the unfilled matrix (see Fig. 6a) – however, as expected the influence increased with increasing temperature as the stiffer nanotubes had much larger effect on the stress amplification when combined with a more rubbery matrix. Finally, an increase in the processing temperature resulted in the decrease of averaged stresses in the nanotube phase as shown in Fig. 6b – this suggests that the interaction between nanotubes and the nanocomposite matrix, and thus the stress transfer, are reduced by the increasing temperature and the softening of the polymeric matrix.

4. Conclusions

A nonlinear multiscale model for simulations of PET/MWCNT nanocomposites in their quasi-solid state was presented in this work. The model connected the representative morphology scale with the macroscopic level through the 3D RVE-based approach and numerical homogenisation. Each RVE was represented through a random dispersion and distribution of MWCNT, approximated as effective nanofibres, and embedded in an elasto-viscoplastic polymeric matrix of PET. The approach predicted not only the macroscopic

stress-strain curves for PET/MWCNT nanocomposites near the glass transition, but also captured separate stress-strain contributions from the matrix and nanotubes.

Enhancements in the uniaxial stress-strain behaviour were predicted as a function of the nanotube loading using the model. The nano-reinforcement effect increased with the applied strain. For the nanotubes perfectly bonded to the matrix the MWCNT phase was predicted to carry the stress, which is around two orders of magnitude larger than the one carried by the matrix. The predicted enhancement in the quasi-solid response of the nanocomposite with the increased nanotube loading, corresponds well to the experimental data in the literature. A significant influence of the processing temperature on the nanocomposite was also predicted – a small change in the processing temperature of 5 °C (within the investigated range 90 °C – 105 °C) was found to reduce the stresses more than twice.

Acknowledgements

Financial support from the EU through the Horizon 2020 Maria Skłodowska-Curie RISE project '*Biaxial stretching of PLLA-WS2 nanocomposites for thinner and stronger biomedical scaffolds*' (*Bi-Stretch-4-Biomed*) (691238) is gratefully acknowledged.

References

[1] R.S. Rajeev et al., *European Polymer Journal*, 45: 967-984, 2009.

[2] Y. Shen et al., *Composites Science and Technology*, 71: 758-764, 2011.

[3] B. Mayoral et al., *RSC Advances*, 3: 5162-5183, 2013.

[4] A. Adams et al., *Polymer*, 41: 771-786, 2000.

[5] M.C. Boyce et al., *Polymer*, 41: 2183-2201, 2000.

[6] L. Chevalier et al., *Mechanics of Materials*, 52: 103-116, 2012.

[7] P.E. Spencer et al., *Mechanics of Time-dependent Materials*, 12: 313-327, 2008.

[8] Ł. Figiel et al., *Modelling and Simulation in Materials Science and* Engineering, 18 (015001), 2010.

[9] C. Pisano, Ł. Figiel, *Composites Science and Technology*, 75: 35-41, 2013.

[10] D. Weidt, Ł. Figiel, *Composites Science and Technology*, 115: 52-59, 2015.

[11] L. Shen, J. Li, *Physical Review B*, 69(4): 45414.

[12] L. Shen, J. Li, *Physical Review B*, 71(3): 35412, 2005.

[13] N. Hu et al. *Proceedings of the Royal Society London A*, 461: 1685-1710, 2005.

[14] Ł. Figiel, *Computational Materials Science*, 84: 244-254: 2014.

[15] N. Hu et al. *Composites Science and Technology*, 60: 1811-1823, 2000.

[16] D. Weidt, Ł. Figiel, *Computational Materials Science*, 82: 298-309, 2014.